Nanomedicine: Nanotechnology, Biology, and Medicine
13 (2017) 1205–1217

nanomedicine
Nanotechnology, Biology, and Medicine

nanomedjournal.com

Nano-analyses of wear particles from metal-on-metal and non-metal-on-metal dual modular neck hip arthroplasty

Zhidao Xia, PhD[a,*], Benjamin F Ricciardi, MD[b], Zhao Liu, BA, MSc[a], Christopher von Ruhland, PhD[c], Mike Ward, PhD[d], Alex Lord, PhD[a], Louise Hughes, PhD[e], Steven R. Goldring, MD[f], Edward Purdue, PhD[f], David Murray, MD, FRSC[g], Giorgio Perino, MD[h]

[a]*Centre for Nanohealth, Swansea University Medical School, Swansea, UK*
[b]*Hospital for Special Surgery, Department of Orthopedic Surgery, New York, USA*
[c]*Electron and Light Microscopy Facility, Central Biotechnology Services, School of Medicine, Cardiff University, Cardiff, UK*
[d]*Leeds Electron Microscopy and Spectroscopy Centre, Institute for Materials Research, School of Chemical and Process Engineering, University of Leeds, UK*
[e]*Bio-Imaging Unit, Department of Biological and Medical Sciences, Oxford Brookes University, Oxford, UK*
[f]*Hospital for Special Surgery, Division of Research, New York, USA*
[g]*Nuffield Department of Orthopaedics, Rheumatology and Musculoskeletal Science, University of Oxford, Oxford, UK*
[h]*Hospital for Special Surgery, Department of Pathology and Laboratory Medicine, New York, USA*

Received 6 May 2016; accepted 17 November 2016

Abstract

Increased failure rates due to metallic wear particle-associated adverse local tissue reactions (ALTR) is a significant clinical problem in resurfacing and total hip arthroplasty. Retrieved periprosthetic tissue of 53 cases with corrosion/conventional metallic wear particles from 285 revision operations for ALTR was selected for nano-analyses. Three major classes of hip implants associated with ALTR, metal-on-metal hip resurfacing arthroplasty (MoM HRA) and large head total hip replacement (MoM LHTHA) and non-metal-on-metal dual modular neck total hip replacement (Non-MoM DMNTHA) were included. The size, shape, distribution, element composition, and crystal structure of the metal particles were analyzed by conventional histological examination and electron microscopy with analytic tools of 2D X-ray energy dispersive spectrometry and X-ray diffraction. Distinct differences in size, shape, and element composition of the metallic particles were detected in each implant class which correlate with the histological features of severity of ALTR and variability in implant performance.

Key words: Hip arthroplasty; Adverse local tissue reaction (ALTR); Metal-on-metal hip resurfacing arthroplasty (MoM HRA); Metal-on-metal large head total hip replacement (MoM LHTHA); Non-metal-on-metal dual modular neck total hip replacement (non-MoM DMNTHA)

Abbreviations: ALTR, adverse local tissue reaction; ALVAL, aseptic lymphocytic vasculitis associated lesion; ARMD, adverse reaction to metallic debris; BSEM, backscatter scanning electron microscopy; DMN, Dual modular neck; EDS, energy-dispersive X-ray spectroscopy; H-E, hematoxylin and eosin staining; MoM, metal-on-metal; MoM HRA, metal-on-metal hip resurfacing arthroplasty; MoM LHTHA, metal-on-metal large head total hip arthroplasty; Mϕ, macrophages; NJR, National Joint Registry for England Wales and Northern Ireland; NJRR, National Joint Replacement Registry of the Australian Orthopedic Association; Non-MoM DMNTHA, non-metal-on-metal hip dual modular neck total hip arthroplasty; SDD, silicon drift detector; SEM, scanning electron microscopy; TEM, transmission electron microscopy; XRD, x-ray diffraction spectrometry.

*Corresponding author.
E-mail address: zhidao.xia@gmail.com (Z. Xia).

Total hip arthroplasty (THA) has been the most successful operation to relieve pain and restore mobility from osteoarthritis for over four decades; however, implant wear-related complications remain a concerning cause of early failure. In the past decade, a new generation of metal-on-metal (MoM) bearing surface hip implants was developed with the rationale of reducing the complications due to polyethylene wear and hip dislocation.[1–4] The most common implant designs utilizing this bearing surface were the MoM hip resurfacing arthroplasty (MoM HRA), designed with the rationale of preserving more femoral bone and providing a greater range of motion than conventional THA,[5,6] and the large head (>36 mm diameter)

http://dx.doi.org/10.1016/j.nano.2016.11.003

metal-on-metal total hip arthroplasty (MoM LHTHA) with the rationale of reducing the rate of hip dislocation. The use of larger metallic heads in the MoM LHTHA implant class lead to the use of an additional metal-on-metal interface between the head and neck taper surfaces, which in the majority of implants was a cobalt chromium (CoCr) metallic adapter sleeve. A class of non-MoM THA implants utilizing a metal-on-metal interface at the neck male taper-stem junction, predominantly a CoCr dual modular neck (Non-MoM DMNTHA), was also introduced with the rationale of providing customization of neck length, offset, and version.[7–9]

It has been reported that more than 1 million MoM hip implants, either THA or HRA, have been implanted worldwide with large heads used in the majority of cases.[10] Data provided by the National Joint Registry for England, Wales and Northern Ireland (NJR) from April 1 to December 31, 2013, show that 10.9% of all hips implanted over this period were MoMLHTHA and MoM HRA with a peak period between 2005 and 2009. In the United States, data from the Nationwide Inpatient Service showed that 38,754 implants (34.6%) were of MoM bearing surface out of a total of 112,095 implants used for primary hip arthroplasty from October 1, 2005, to December 31, 2006, excluding MoM HRA.[11,12]

The unintended consequence of this generation of implants was the occurrence of severe inflammatory reactions of the periprosthetic soft tissues. In particular, increased rates of early reactions were reported across a diverse spectrum of implant configurations due to increased risk of corrosion and wear.[13–17] These failures can result in extensive tissue necrosis, injury to abductor muscles and tendons, aseptic loosening/osteolysis, increased revision complications, and significant patient morbidity.[15,18–20]

Data from the NJR and the NJRR reported increased revision rates for MoM hip implants due to wear-related complications.[21] The impact on public health and on the health care costs are already considerable and will grow substantially in the next decade, considering the large number of patients implanted and the follow-up needed for lifespan of the implant and also after implant revision to monitor for adverse long-term effects.[22]

The histopathological characterization of the periprosthetic adverse reactions has evolved from the original description of aseptic lymphocytic vasculitis associated lesion (ALVAL), characterized by a pseudo-capsular and neo-synovial mass (pseudotumor) containing a macrophagic infiltrate filled with cytoplasmic inclusions of wear products of uncertain composition admixed with a dense perivascular lymphocytic infiltrate and a variable amount of soft tissue necrosis[23] to a more complex picture defined as adverse local tissue reaction (ALTR) or adverse reaction to metallic debris (ARMD), exhibiting a variety of histological patterns.[24–26]

The lymphocytic component associated with the presence of a layer of soft tissue necrosis of variable thickness is characteristic of this type of reaction, and has been attributed to a hypersensitivity type IV reaction to wear debris produced at the MoM interfaces.[27,28] However, metal hypersensitivity is unlikely to explain many of these cases, as the occurrence of ALTR is much higher than its incidence in the general population. The association of corrosion products with the adverse reaction has been well documented in analyses of retrieved implants[14,29,30] and histological characterization studies[24–26,31–33]; however, only a few reports have been published on the composition of wear particles generated at the MoM surfaces.[31,34–36] The importance of wear particle shape, chemistry, surface properties, and retention has been emphasized[37] and more comprehensive studies have been advocated by the European Union *ad hoc* scientific committee.[38]

The main difficulty in understanding the mechanisms of adverse reactions to the particulate wear of metal-on-metal interfaces is that the wear products are at the nanometer scale and cannot be properly assessed with conventional examination by light microscopy. The application of techniques used in materials science, in particular analytical electron microscopy for material characterization, has been successful in providing remarkable information regarding materials within cells and extracellular matrix, such as the structure and composition of human cardiovascular tissue particulate calcification[39] and we used it for this analysis.

We tested two hypotheses: (1) Different classes of hip implants generate wear debris of different physical and chemical characteristics, which can affect either the quantitative and/or the qualitative aspects of the inflammatory response observed in the ALTR; (2) The characteristics of wear debris are consistent in all tested samples of each implant class.

Methods

Three hip implant classes were selected: 1. MoM HRA; 2. MoM LHTHA with CoCr metallic adapter sleeve; 3. Non-MoM DMNTHA with CoCr DMN. The configurations of the three implant classes and the different sources of metallic particulate wear are provided in Figure 1.

A combination of techniques was used for particle identification and analysis.

Histological analysis of revision tissues

Periprosthetic tissues were collected at surgery from June 2011 to December 2014 for a total of 285 cases which underwent revision surgery for adverse local tissue reaction (ALTR) at a single institution. All patients provided informed, written consent regarding participation in this study. Ethical committee approval was obtained prior to this study (Institutional Review Board, Hospital for Special Surgery, Protocol Number 26085). Out of the 285 collected cases in the study time period for which routine histological examination was performed and previously reported,[40] 53 cases provided viable macrophagic infiltrate with particle content suitable for electron microscopy analysis.

The implant group composition and manufacturer were as follows: 12 MoM HRA (Birmingham Hip Resurfacing, Smith and Nephew, London, UK); 18 MoM LHTHA (femoral head >36 mm diameter) with metallic CoCrMo sleeve adapter (15 Birmingham Hip Replacement, Smith and Nephew, London, UK; 3 ASR Hip Replacement, Depuy/Synthes, Warsaw, IN) and 23 non-MoM DMNTHA with CoCr dual modular neck (22 Rejuvenate, Stryker, Kalamazoo, MI and 1 ABGII, Stryker, Kalamazoo, MI).

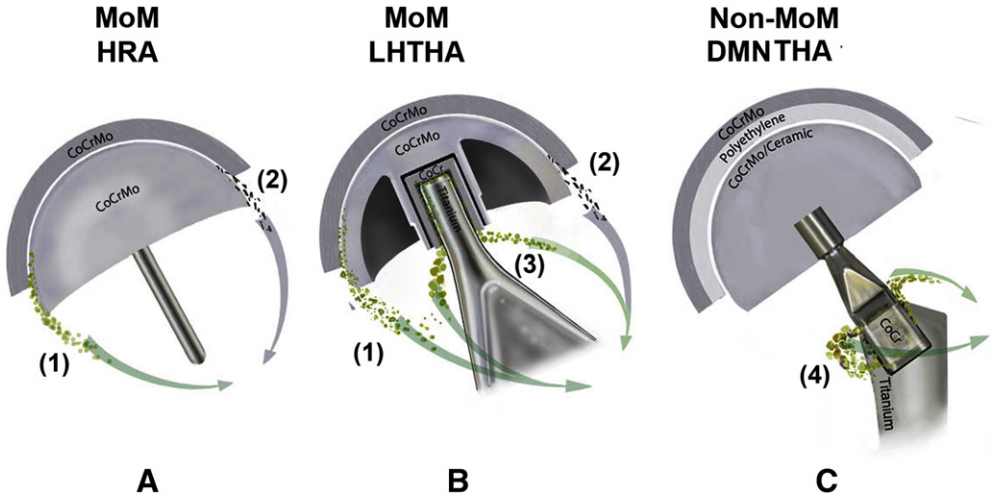

Figure 1. Three common classes of hip implants associated with ALTR.**A**, Metal-on-metal hip resurfacing arthroplasty (MoM HRA). Metallic particles are produced at the bearing surface by sliding tribocorrosion (1) and edge loading (2). **B**, Metal-on-metal large head total hip arthroplasty (MoM LHTHA). Metal particles are produced at the bearing surface by sliding tribocorrosion (1) and edge loading (2), and at the metallic stem and metallic adapter sleeve interface by fretting and crevice corrosion and possibly abrasion (3). **C**, Non-MoM bearing surface (metal-on-polyethylene or ceramic-on-polyethylene) THA with Co/Cr/Mo metallic dual modular neck (Non-MoM DMNTHA), where metallic particles are produced by fretting and crevice corrosion at the neck/stem interface (4).

The tissue was collected fresh from several areas around the implant with MRI guidance when available and placed immediately on ice.

Paraffin embedding and sectioning

Collected tissues were fixed in 10% neutral buffered formalin after frozen section examination, extensively sampled at macroscopic examination, processed, paraffin-embedded, and cut at 5 μm for H-E staining. Histological analysis was performed according to a previously reported protocol.[26] Sections were examined with a Zeiss Axioskop 40 microscope and images captured digitally using a ProgRes camera (Jenoptik, Germany).

Resin embedding and sectioning

Fresh periprosthetic tissue was examined macroscopically and a frozen section of the most viable sample was performed in each case for cell analysis with presence of macrophages with particle content. When suitable, a thin tissue slice adjacent to the one selected for frozen section was immediately fixed in 2.5% glutaraldehyde for 24 hours and after trimming with preservation of tissue orientation transferred to sodium cacodylate buffer 0.1 M, pH 7.4 at 4 °C. Samples of 1 mm thickness were post-fixed in 2% uranyl acetate, fully dehydrated through graded propan-2-ol (15 minutes each in 50%, 70%, 90%, 2 × 100%), infiltrated with LR White acrylic resin (30 minutes each in 50% LR White in propan-2-ol, 4 × LR White) and polymerized at 50 °C for 24 hours. Osmium post-fixation and uranium and lead staining of sections were omitted to maximize contrast between wear particles and the tissue background.

Light microscopy examination

0.35 μm thick sections were stained with 0.1% toluidine blue in borax buffer. Sections were examined with an Olympus BX51 research light microscope (Olympus Optical Co Ltd., London, U.K.) and images captured with a Zeiss Axiocam digital camera and Axiovision software (Carl Zeiss Vision GmbH, Hallbergmoos, Germany).

Scanning electron microscopy (SEM), backscatter scanning electron microscopy (BSEM), and BSEM-energy-dispersive X-Ray spectroscopy (EDS) element mapping examination

For SEM examination, 0.5mu thick sections were collected onto 5 × 5 mm silicon wafers (Elektron Technology, Essex, UK). The sections were analyzed by SEM (Hitachi S4800, Hitachi Europe Ltd., Berkshire, UK) with backscatter electron imaging and EDS (Oxford Instruments, Oxfordshire, UK).

Transmission electron microscopy (TEM), TEM-EDS element mapping, and X-Ray diffraction spectrometry (XRD) examination

For TEM examination, 100 nm thick sections were collected onto 150 mesh formvar/carbon-coated gold grids and coated with a few nanometer layer of evaporated carbon to eliminate charging.

For metal particle morphology, the samples were observed by TEM (Hitachi A-7650 tomographic transmission EM, Hitachi Europe Ltd., Berkshire, UK) using 100 kV. Images were collected using an AMT 2k62k CCD camera (Advanced Microscopy Technologies, Bury St. Edmunds, Suffolk, UK).

TEM-EDS mapping was carried out using a probe approximately 10 nm in diameter and with the sample tilted 15° towards the detector in a FEI Tecnai F20 200 kV FEGTEM (FEI Company, Oregon, USA) fitted with an Oxford Instruments 80 mm^2 EDX Silicon Drift Detector (SDD) and running INCA software.

Statistical analysis

All histological variables were compared across the three implant classes. Continuous variables were assessed using one-way ANOVA and the Kruskall-Wallis test was used for

Table 1
Demographic data from the three implant classes (mean ± SE).

Implant class		MoM HRA	MoM LHTHA	Non-MoM DMNTHA
Cases		12	18	23
Gender	Male	6	11	12
	Female	6	7	11
Age		56.83 ± 2.41	62.40 ± 0.88	62.87 ± 2.00
Implant time (months)		51.58 ± 7.80*	59.85 ± 1.52*	30.88 ± 2.51*
Symptom duration (months)		16.91 ± 5.54	12.78 ± 1.11	9.95 ± 3.17
Head size (mm)		44.67 ± 1.76	43.68 ± 0.76	30.17 ± 0.81
Blood metal Ions (ppb)	Co	36.00 ± 13.58 (n = 10)	28.00 ± 10.92 (n = 10)	9.48 ± 1.35 (n = 18)
	Cr	41.40 ± 16.20 (n = 10)	17.00 ± 6.58 (n = 10)	1.69 ± 0.34 (n = 18)

MoM LHTHA ($p < 0.001$) groups.
* The Non-MoM DMNTHA group had shorter implant time than the MoM HRA ($p < 0.001$) and the MoM LHTHA ($p < 0.001$) groups.

Table 2
Significant differences in histological findings from 53 cases and 285 cases from the three implant classes and correlation with particle analysis[(a)].

Histological finding		MoM HRA	MoM LHTHA	Non-MoM DMNTHA
Soft tissue necrosis	**N = 53**	**NA**	**NA**	**NA**
	N = 285	11*	32*	53*
Macrophage distribution (% Grade 1, Grade 2, Grade 3)	**N = 53**	**0, 8, 92****	**0, 33, 67****	**13, 9, 78****
	N = 285	0, 5, 95**	1, 34, 65**	7, 51, 42**
Lymphocyte distribution (% Grade 0, Grade 1, Grade 2, Grade 3 + 4)	**N = 53**	**27, 18, 27, 28^**	**5, 15, 45, 35^**	**0, 0, 30, 70^**
	N = 285	39, 25, 18, 18^	11, 25, 31, 33^	6, 7, 29, 58^
Histological pattern (% 0, 1, 2, 3)	**N = 53**	**27, 63, 8, 0**	**10, 45, 30, 10**	**0, 43, 35, 22**
	N = 285	41, 48, 11, 0	11, 62, 22, 5	6, 46, 32, 16
Particle analysis				
Size	Nano-	<10 nm; 10–800 nm	<10 nm; 10–2250 nm	<10; rare; 10–400 nm
	Micro-	Not present	1–30 μm	1–30 μm
Shape	Morphology	Circular, irregular, small needle-like	Circular, irregular, small and large needle-like	Circular nanoparticles and large agglomerations
	Feret ratio (6 cases/group)	1.799# ± 0.046	2.079# ± 0.119	1.642# ± 0.040
Composition		Cr > > Co, Mo, P, O	Cr > Co, Mo, Ti, V, P, O Non co-localized	Cr, Co, Mo, Ti, V, P, O Co-localized

All values for soft tissue necrosis, cell distributions, and histological patterns are expressed as percentage of cases with each morphologic feature. Histological patterns are: 0 = macrophagic only, 1 = mixed macrophagic and lymphocytic, 2 = mixed macrophagic and lymphocytic with germinal centers/eosinophils, 3 = granulomatous). Values in bold are from the current series of 53 cases, the others from the full cohort of 285 cases previously reported.[40]
[a] From reference [40], modified.
* The MoM HRA group had significantly lower percentage of cases with soft tissue necrosis than the MoM LHTHA ($p = 0.009$) and Non-MoM DMNTHA ($p = 0.007$) groups.
** The MoM HRA group had significantly higher percentage of cases with grade 3 macrophagic infiltrate than the MoM LHTHA (**$p = 0.40$**; $p = 0.007$) and Non-MoM DMNTHA (**$p = 0.40$**; $p = 0.007$) groups.
^ The Non-MoM DMNTHA group had significantly higher percentage of cases with high grade lymphocytic distribution than the MoM HRA (**$p = 0.01$**; $p = 0.007$) and the MoM LHTHA (**$p = 0.01$**; $p = 0.007$).
# The Non-MoM DMNTHA group had significantly more circular nanoparticles compared with MoM LHTHA ($p = 0.01$) and MoM HRA ($p = 0.03$).

non-parametric data. Caterogical data was compared using the chi-square test. Histological patterns amongst the different implant classes were compared using the Fischer's exact test. Bonferroni correction was used for pairwise comparisons of histological data adjusted for multiple comparisons.

Results

Our hypotheses were tested by in depth analysis of periprosthetic hip joint tissues retrieved at implant revision from 53 patients with confirmed histological evidence of ALTR. Demographic data and blood levels of cobalt (Co) and chromium (Cr) are provided in Table 1; wear particle characteristics with histological correlation are shown in Table 2.

Differences in quantitative and qualitative analysis of wear particles were observed in H-E stained sections (Figure 2, *A*, *C* and *E*). The histological findings were confirmed by examination of toluidine blue-stained semi-thin resin sections, which provided more detailed morphological definition of the wear particles (Figure 2, *B*, *D* and *F*). Macrophages present in the retrieved tissues from MoM-HRA (Figure 2, A and B) and MoM-LHTHA (Figure 2, C and D) groups were filled with phagosomes containing minute particles, previously described as wear-related cytoplasmic inclusions.[23] The MoM-LHTHA group showed also irregular particles presumably resulting

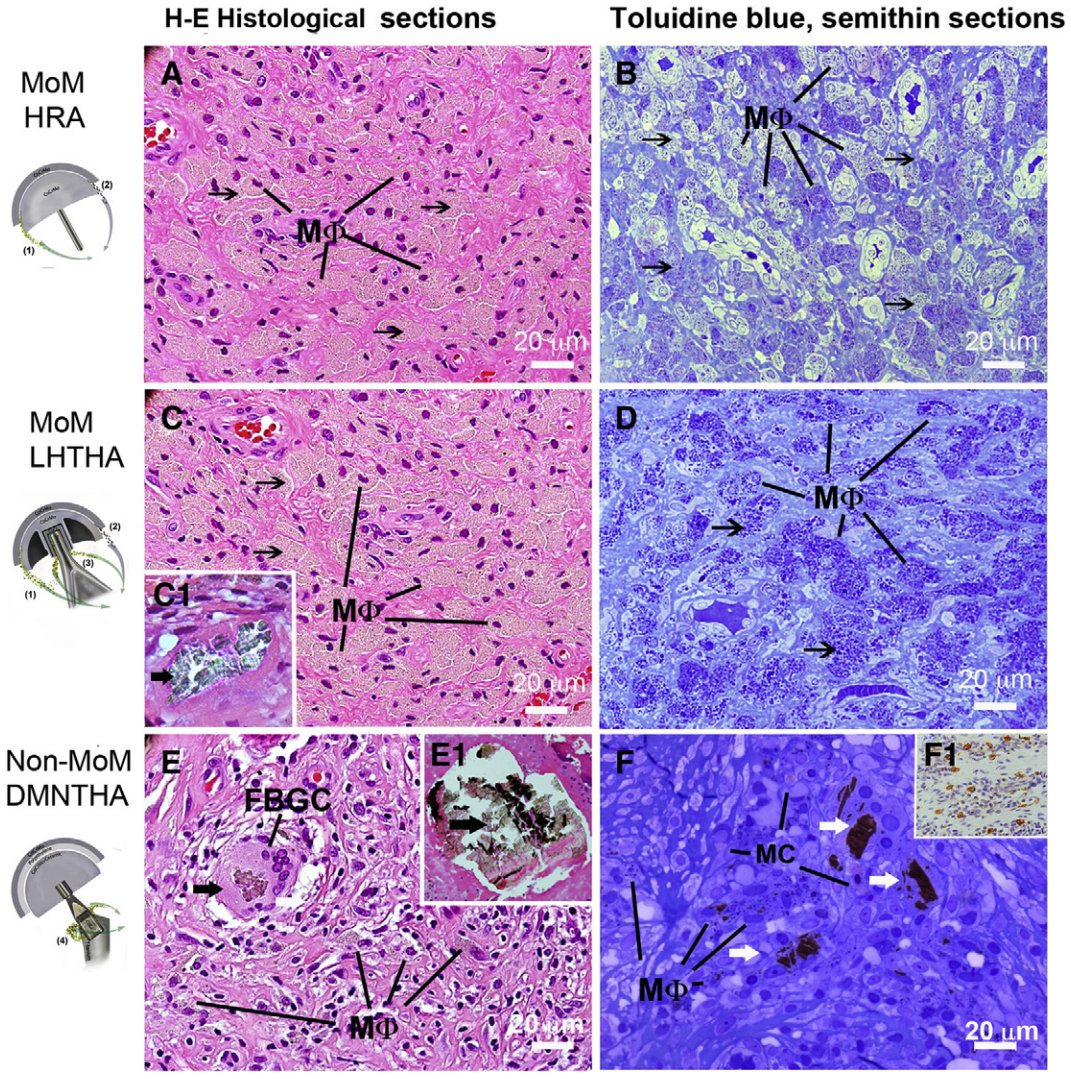

Figure 2. Microphotographs of histological sections (**A, C, E**) and semi-thin sections (**B, D, F**) from the three classes of hip arthroplasty. **A**, MoM HRA group: fine globular greenish particle aggregates (short arrows) fill the macrophages (Mϕ). **B**, The wear metal particles (short arrows) are more evident. **C**, MoM LHTHA group: fine globular and irregular greenish particle aggregates (short arrows) fill the macrophages (Mϕ) and a large greenish particulate aggregate present in another section is shown in inset C1 (short thick arrow). **D**, The variability in size of the particle aggregates (short arrows) in the macrophages (Mϕ) is evident with predominant globular and occasional irregular shape. **E**, Non-MoM DMNTHA group: aggregates of corrosion particles (short thick arrow) in the foreign body multinucleated giant cell (FBGC) and macrophages (Mϕ) and a large greenish-reddish-black particulate aggregate present in another section is shown in inset E1 (short thick arrow). **F**, The breakdown of a large particulate aggregate is more evident with engulfment of larger fragments in the FBGCs (thick white arrows) and of smaller fragments in the macrophages (Mϕ) with interspersed numerous mast cells (MC), positive for CD117 as shown in inset F1.

from the fragmentation of larger particles and/or larger particle aggregates (Figure 2, *C*, inset). In the non-MoM DMNTHA group, macrophages contained only scattered, irregular nano-size particle aggregates (Figure 2, E and F) also presumably derived from the fragmentation of larger aggregates (Figure 2, E, inset). Toluidine blue staining allowed the identification of mast cells detected by metachromasia of the cytoplasmic granules which were numerous in the THA cases and especially in some tissue samples of the Non-MoM DMNTHA group (Figure 2, *F*), positive for CD117 (Figure 2 F, inset).

Nanoscale morphological analysis was performed by electron microscopy examination. The unstained ultrathin sections were examined by TEM and the unstained semi-thin sections were examined by BSEM (Figure 3). All wear nanoparticles were electron dense with variable intensity by TEM and the majority of the particles from all implants were at the nanometer scale, with a small proportion of particle aggregates at the micrometer scale. The particles were stored in the phagosome complex (Figure 3, *B* and *D1*), which is consistent with findings from a previous study.[36] Particle aggregates ranging in size from 1 to 20 µm were also detected in multinucleated foreign body giant cells (Figure 3, *D2* and *F*). Free-form wear particles were observed in stromal tissue or in exfoliated, superficial necrotic cellular debris.

The differences in the characteristics of the wear particles from the three classes of hip implants were evident when examined at the nanometer scale (Figure 3). In MoM HRA group they were mainly less than 50 nm in size, circular or irregular and

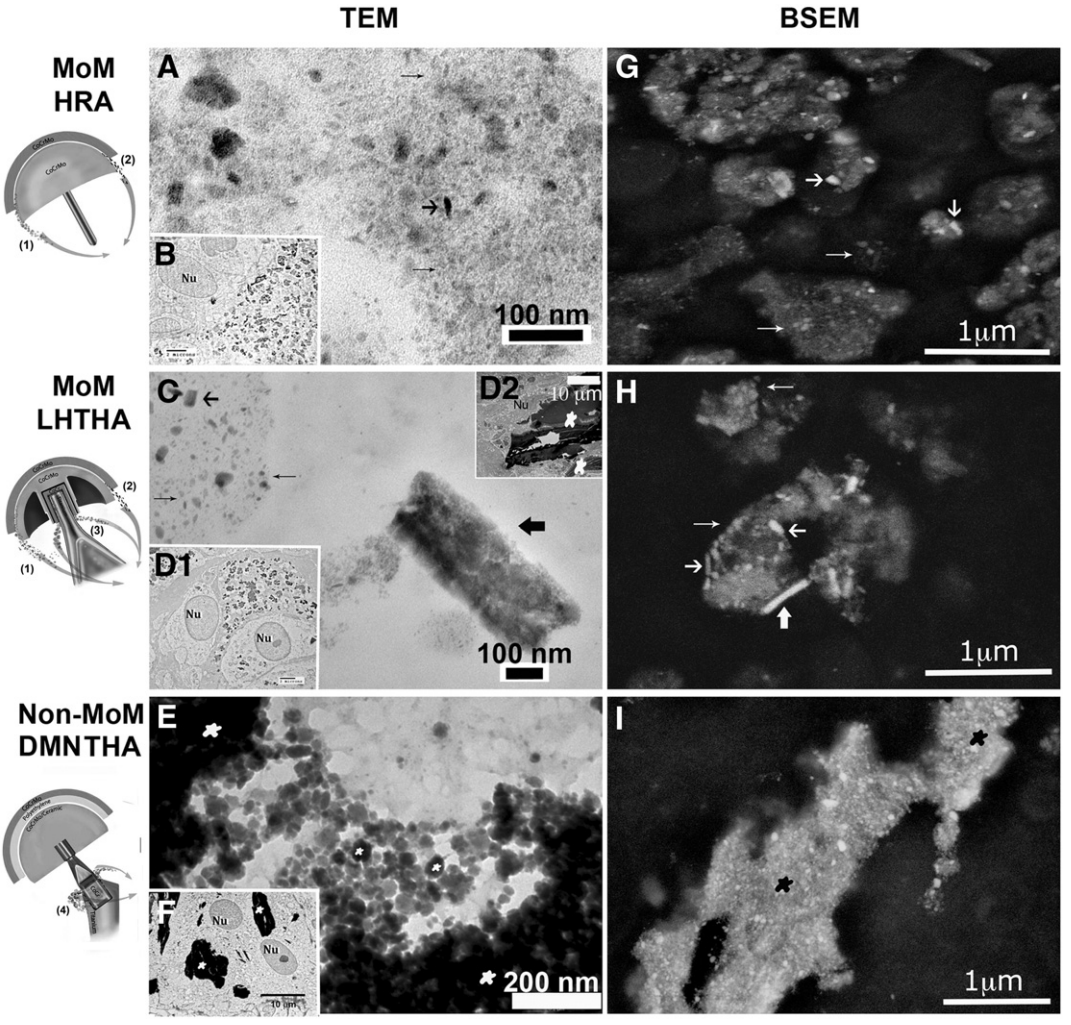

Figure 3. Micrographs of typical wear particles in unstained ultrathin sections examined by TEM (**A**–**F**) and unstained semi-thin sections examined by BSEM (**G**–**I**) from the three classes of hip arthroplasty. **A**, MoM HRA group: a large majority of low electron density circular and cloudy nanoparticles (thin long arrows) and a small number of electron density needle-like particles (thick short arrow) are present. The majority of particles are less than 50 nm in size, shown in a macrophage in inset **B** (Nu, nucleus). **C**, MoM LHTHA group: combination of two types of wear particles, small circular around 50 nm in size of low electron density (thin long arrows) and larger of variable shape and size of high electron density (thick short arrow), in this case up to 1.9 μm (thick short arrow in bold). Nano-size particles in macrophages in inset **D**1 (Nu, nucleus) and micron-size particles in a giant cell (white stars) in inset **D**2. **E**, Non-MoM DMNTHA group: aggregates of high electron density nanoparticles (white stars) ranging from 10 to 150 in macrophages in inset F (Nu, nucleus). **G**, MoM HRA group: cloudy nanoparticles (thin long arrows) and high electron density needle-like particles (thick short arrows) as seen in **A** and inset **B**. **H**, MoM LHTHA group: cloudy nanoparticles (thin long arrows), irregular particles (thin short arrows) and highly electron dense needle-shaped wear particles (thick short arrow) as seen in **C** and inset **D**. **I**, Non-MoM DMNTHA group: large amount of agglomeration of circular nanoparticles (black stars) as seen in **E** and inset **F** (white stars).

of low electron density. A large percentage of these particles were amorphous and smaller than 10 nm and were present in the phagosomes (Figure 3, *A* and *G*) admixed with a small number of larger, high electron density needle-like particles (Figure 3, *A and G*).

The wear particles in the MoM-LHTHA group exhibited greater variability in size than those described in the MoM HRA group: circular or irregular low electron density particles at the size below 100 nm (Figure 3, *C and H*) were admixed to numerous larger irregular and needle-like high electron density particles (Figure 3, *C* and *H*) ranging from 100 nanometers to a few micrometers in some cases.

The wear particles in the non-MoM DMNTHA group showed distinct differences in comparison to the MoM-HRA and MoM-LHTHA wear products. They were an agglomeration of circular high electron density particles sized between 10 and 100 nm (Figure 3, *E* and *I*) with only occasional particles less than 10 nm in size, embedded in a matrix of intermediate electron density, higher than the background tissue but lower than the wear particles (Figure 3, *E* and *I*).

Measurements of particle sizes by BSEM are not as accurate as those produced by TEM (Figure 3, *G*, *H* and *I*). However, the morphological profiles of the wear particles of the three configurations by BSEM were consistent with the TEM findings.

Six samples of each implant class were selected for quantification of the number, size and shape of the particles using ImageJ software. The total number was to some extent difficult to determine with accuracy since the particles sized

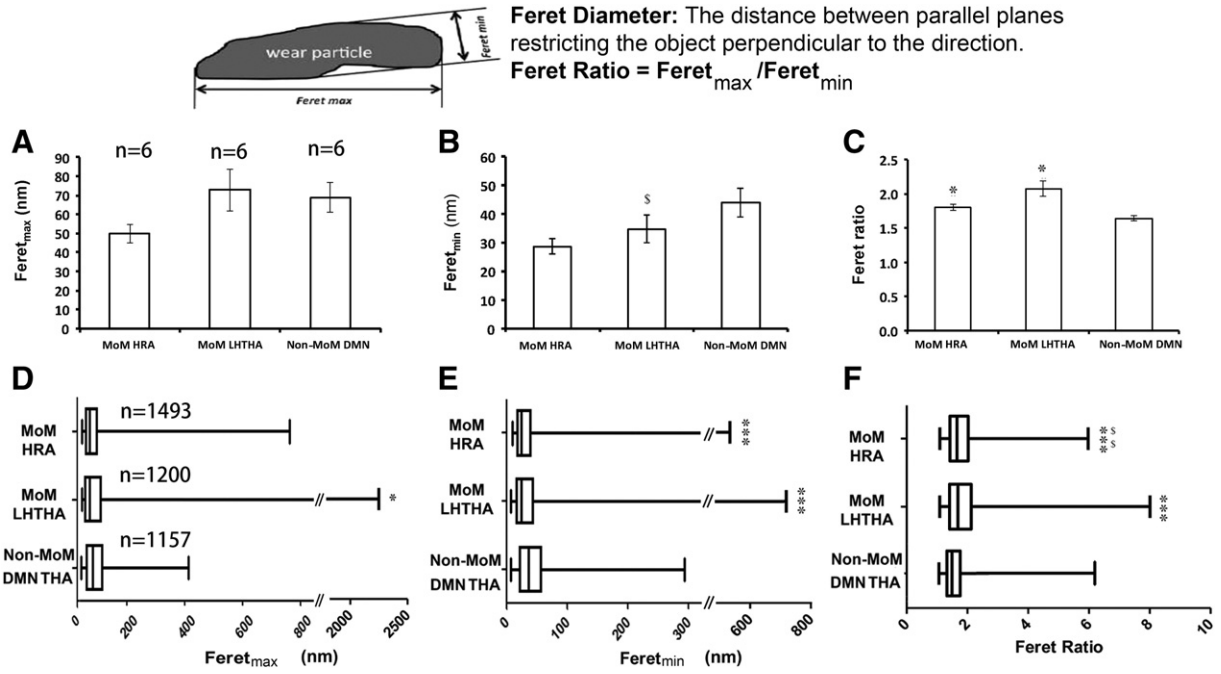

Figure 4. Morphometric analysis of nanoparticles of six samples from the three classes of hip arthroplasty (particles with at least one Feret diameter larger than 10 nm). **A**, The diagram of the measurement of Feret diameters and their definition; **B**–**D** shows the range of particle sizes (**B**, Feret max and **C**, Feret Min) and shapes (Feret ratio) distribution of the three classes of hip implants.

between 1 and 10 nm can be subject to the quantum confinement effect. Therefore the size of the particles was defined in terms of Feret diameters; only particles that had at least one Feret diameter larger than 10 nm were included in this analysis. The shape of the particles released from the three classes of hip implants was defined by the Feret ratio as shown in Figure 4. The comparison of the Feret diameters and ratio of the three implant classes is shown in Figure 4, *A-C*. The range of particle size was measured as Feret max (Figure 4, *D*), Feret min (Figure 4, *E*), and as Feret ratio for shape distribution (Figure 4, *F*). The Feret ratio is close to 1 for circular or square particles and its increase corresponds to a progressive elongation of the particles up to a needle-like shape.

The average values for Feret min, Feret max, and Feret ratio for each group are provided in Table 2. The average Feret max of the MoM HRA and the MoM LHTHA groups were significantly lower than those in the Non-MoM DMNTHA group ($p < 0.001$). The average Feret min in the MoM HRA and the MoM LHTHA groups were lower than those in the Non-MoM DMNTHA group ($p < 0.001$). The average Feret ratio of the Non-MoM DMNTHA group was significantly lower than those from the MoM LHTHA ($p = 0.001$) and the MoM HRA ($p = 0.03$) groups.

The results of the element analysis of the wear particles on three samples for each implant class are shown in Figure 5.

High concentration of chromium was detected in samples from all three groups (Figure 5, *A1-I1*). Cobalt was detected only in high electron density particles in the MoM HRA (Figure 5, *A3*, *B3* and *C3*) and MoM LHTHA groups (Figure 5, *F3*), but in all of the Non-MoM DMNTHA samples (Figure 5, *G3*, *H3* and *I3*). A very low concentration of molybdenum was detected in both MoM HRA and MoM LHTHA samples (Figure 5, *A4–F4*), which was higher in the Non-MoM DMNTHA samples (Figure 5, *G4*, *H4* and *I4*). Titanium and vanadium showed variable concentration in the MoM-LHTHA (Figure 5, *D5–F5*, *D6–F6*) and Non-MoM DMNTHA (Figure 5, *G5–I5*, *G6–I6*) groups and were not present in the MoM HRA group (Figure 5, *A5–C5*, *A6–C6*). Iron was detected in some samples (Figure 5, *C7*, *H7* and *I7*) and did not co-localize with other metal particles. Oxygen (Figure 5, *A9–I9*) was associated with phosphorus in all particles (Figure 5, *A8–I8*) and the concentration of phosphorus was lower than oxygen.

Although wear particles from both MoM-LHTHA and Non-MoM DMNTHA groups contained chromium/cobalt/molybdenum/titanium/vanadium, their distribution between these two groups was distinctively different. In the MoM LHTHA group, titanium/vanadium particles were separated from chromium/cobalt particles, whereas in the non-MoM DMNTHA group, titanium/vanadium particles were mixed with chromium/cobalt/molybdenum particles. By overlay of titanium with chromium maps (Figure 6), we observed chromium particles in the MoM HRA group and two types of particles in the samples from the MoM LHTHA group: (1) Highly electron dense large needle-like particles rich in titanium with very low chromium (Figure 6, *B2* and *B3* spectrum 1); (2) Particles containing both chromium and titanium at a ratio very similar to those of the Non-MoM DMNTHA group (Figure 6, *B2* and *B3* spectrum 2). In the Non-MoM DMNTHA group, circular nanoparticles contained chromium and titanium (Figure 6, *C2* and *C3*).

XRD analysis showed that all three samples of the Non-MoM DMNTHA had a crystalline structure composed of Cr_2O_3 whereas those from MoM-HRA and MoM-LHTHA groups had an amorphous structure (See Fig. 7.).

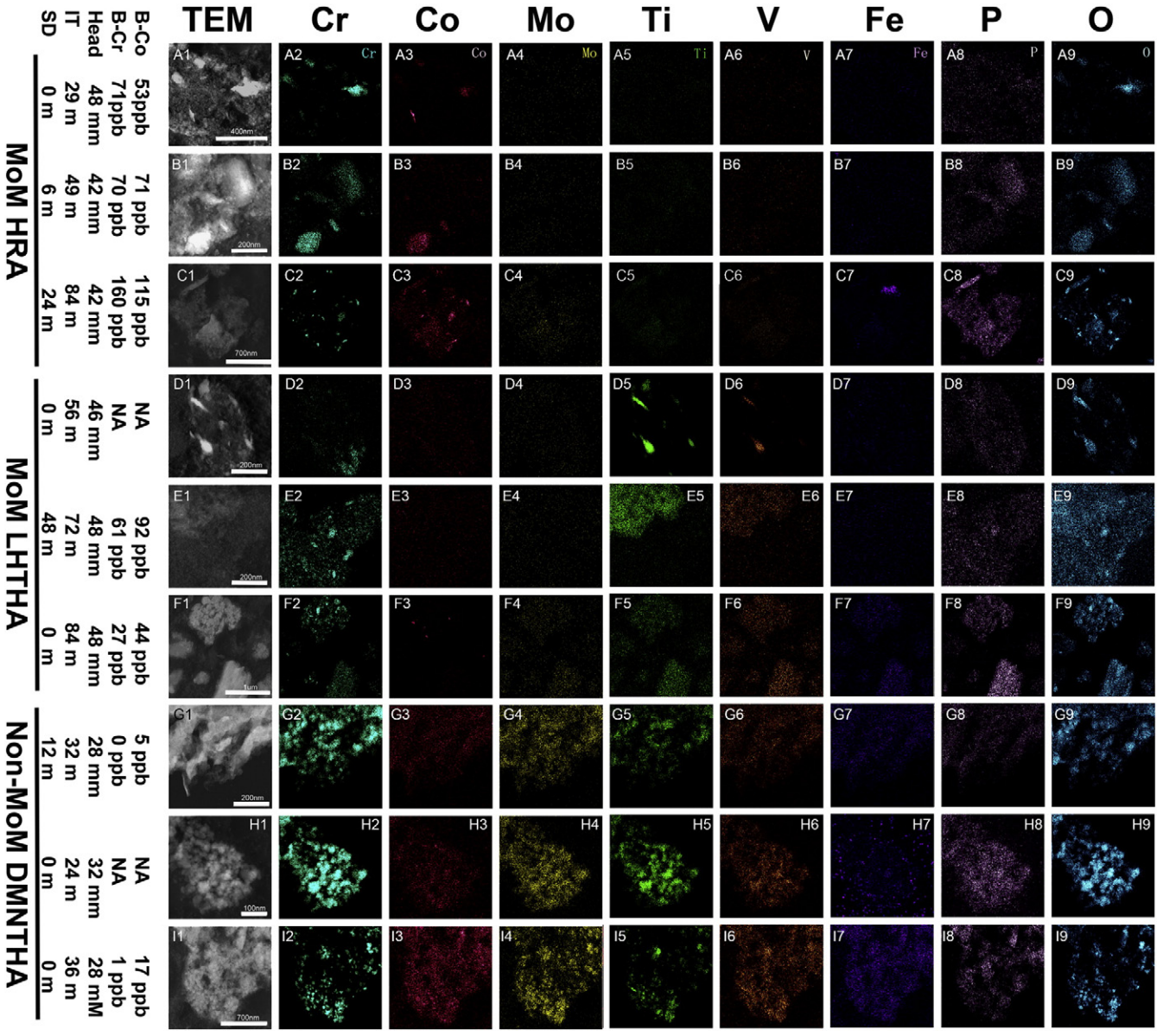

Figure 5. Micrographs of TEM EDS element mapping of three samples of each class of hip arthroplasty. Column A1-I1, TEM micrographs of 9 samples selected for element mapping. All samples contain variable amounts of Cr particles (A2-I2), P (A8-I8) and O (A9-I9). A small number of high electron density particles in the MoM HRA (A3-C3) and the MoM LHTHA (D3-F3) groups, and the particles in the Non-MoM DMNTHA group (G3-I3) contain Co. High concentration of Mo is present in the Non-MoM DMNTHA group (G4-I4) and barely detectable in MoM HRA and MoM LHTHA groups. Ti and V co-exist in the MoM LHTHA (D5-F5, D6-F6) and the Non-MoM DMNTHA (G5-I5, G6-I6) groups but are not detectable in the MoM HRA group (A5-C5, A6-C6). Fe is detected in some samples (C7, H7 and I7) and does not co-localize with other metal particles. P co-exists with O but its concentration is lower than O.B-Cr, blood Cr ion concentration; B-Co, blood Co ion concentration; Head, femoral head size; IT, implant time; SD, symptom duration. Scale bars: B1, D1, E1, G1 = 200 nm; A1 = 400 nm; C1, I1 = 700 nm; F1 = 1000 nm.

A summary of statistically significant morphologic findings of the histological examination and correlation with the particle analysis is provided in Table 2.

The presence of soft tissue necrosis is not applicable in the current series because the selection process excluded necrotic cases for EM analysis but showed an upward trend in the full series of 285 cases with the lowest value in the MoM HRA group (11% of cases) *versus* the MoM LHTHA group (32%, $p = 0.009$) and the Non-MoM DMNTHA group (53%, $p = 0.007$).[40]

The macrophagic infiltrate distribution in the high grade group (grade 3), a parameter indicative of particle total burden/cell necrosis shows a downward trend with the highest value in the MoM HRA group (92%) *versus* the MoM LHTHA group (67%, $p = 0.40$) and the Non-MoM DMNTHA group (78%, $p = 0.40$), more evident in the series of 285 cases with 95% *versus* 65% ($p = 0.007$) and 42% ($p = 0.007$) of cases, respectively.[40]

The lymphocytic infiltrate distribution shows an upward trend for the high grade group (grade 3 + 4 combined) in the current

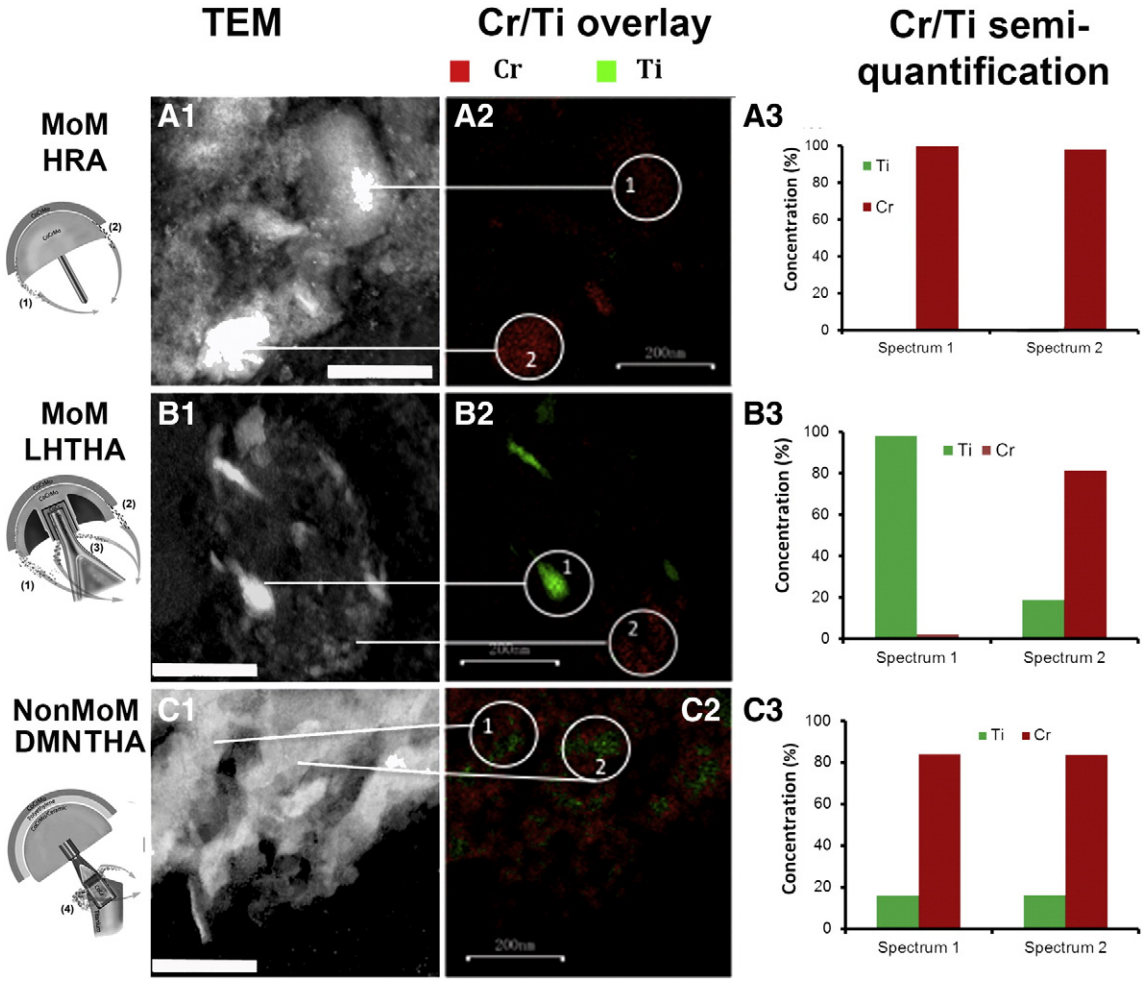

Figure 6. Characterization of the overlaying of two major types of metal particles (Cr and Ti) by semi-quantification of TEM EDS mapping. A1–C1, TEM of typical particles from MoM HRA, MoM LHTHA and Non-MoM DMNTHA groups. A2–C2, Cr and Ti mapping of two particles selected from A1-C1 (in circles). A3–C3, Semi-quantitative analysis of Cr and Ti concentration (%) in two particles. A3, Both particles are composed of Cr without presence of Ti. B3, The two particles show different composition: particle 1 is almost exclusively composed of Ti (98.04%) with minor component of Cr (1.96%) and particle 2 is predominantly composed of Cr (81.31%) with minor component of Ti (18.69%). C3, Both particles show similar composition with predominant Cr element: particle 1 (Cr 84.14%, Ti 15.86%) and particle 2 (Cr 83.72%, Ti 16.28%). Scale bar = 200 nm.

series with the highest value for the Non-MoM DMNTHA group (70% of cases) *versus* the MoM LHTHA group (35%, $p = 0.01$) and the MoM HRA group (28%, $p = 0.01$), and shows similar difference in the larger series of 285 cases with 58%, 33% ($p = 0.007$), and 18% ($p = 0.007$) of cases, respectively.

The histological pattern distribution showed a downward trend of the macrophagic pattern with the highest value in the MoM HRA group (27%) *versus* the MoM LHTHA group (10%) and the Non-MoM DMN THA group (0%) similar to the one observed in the 285 cases series, 41% of the HRA group *versus* 11% of the MoM LHTHA group and 6% of the Non-MoM DMNTHA group and an upward trend either in the mixed macrophagic/lymphocytic group with hypersensitivity features or in the granulomatous pattern, MoM HRA (8% and 0%), MoM LHTHA (30% and 10%) and Non-MoM DMNTHA (35% and 22%) also evident in the series of the 285 cases, MoM HRA (11% and 0%), MoM LHTHA (22% and 5%), and Non-MoM DMNTHA (32% and 16%).

Discussion

Our results showed a distinctive pattern of intracellular particulate material for each of the three classes of implant examined which correlates with the histological analysis of the intensity and severity of the inflammatory reaction as summarized in Table 2. The higher blood levels of Co and Cr ions in the MoM groups compared to the Non-MoM group reported in Table 1 can be explained by the generation of a higher total burden of metallic particles formed at the bearing surface by tribocorrosion and especially edge loading and the longer time of implantation.

In the MoM HRA group, the majority of the wear debris was composed by circular, low electron dense particles smaller than 50 nm and composed of oxidized chromium without detectable cobalt, as previously reported both *in vivo*[35,36] and *in vitro*[41] simulations. These particles are generated by sliding tribocorrosion at the bearing surface[34] and possibly can also represent

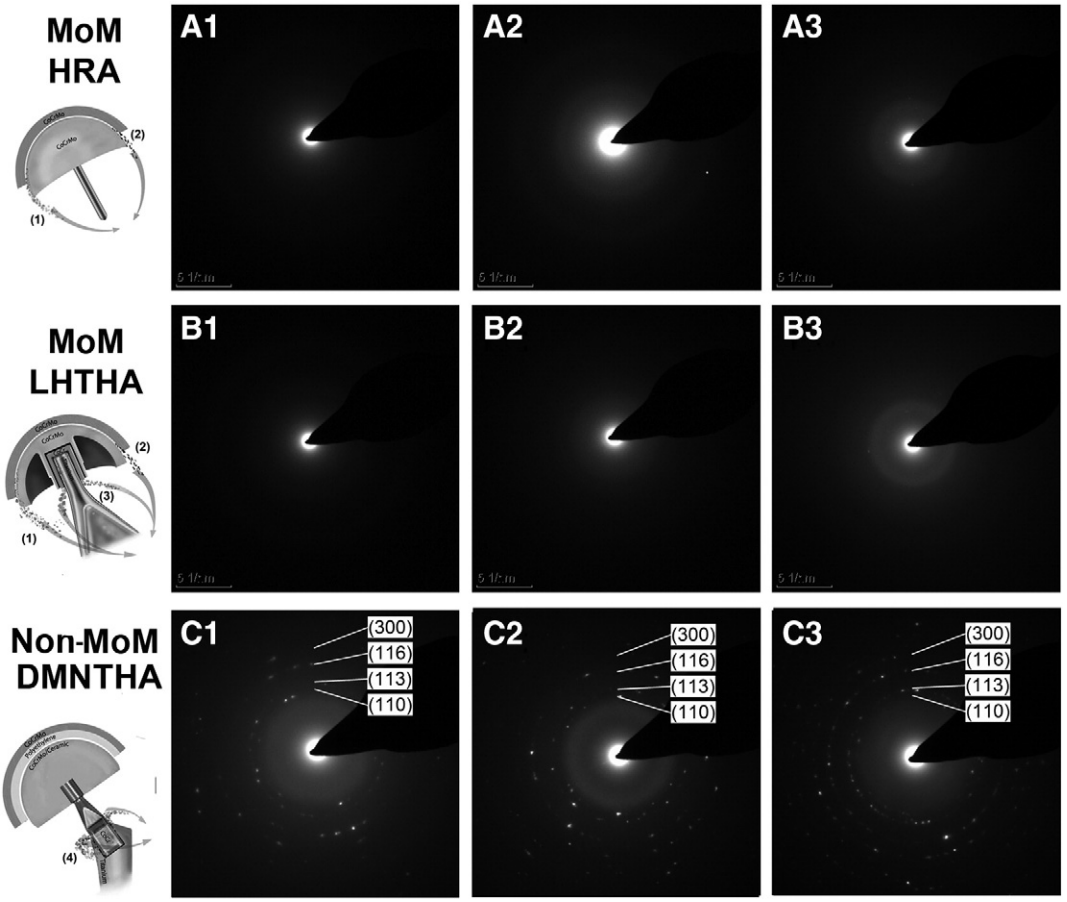

Figure 7. XRD analysis of the crystalline structure of corrosion/conventional metallic particles shown in Figure 5. The three samples from the MoM HRA group (A1–A3) and the MoM LHTHA group (B1–B3) show amorphous structure of the particles; the three samples from non-MoM DMNTHA (C1–C3) show crystalline structure of the particles and the spectra were identified as Cr_2O_3.

secondary particles that are phagocytized after their release by necrotic macrophages. A much smaller, variable number of needle-shaped, highly electron dense particles composed of oxidized chromium and cobalt were also detected, suggesting formation by edge loading or in some cases by gross dislocation/migration of the implant components.

In the MoM LHTHA group the amount and composition of the wear products was more heterogeneous than in the other two groups. In addition to a large number of low electron density nanoparticles similar to those observed in the MoM HRA group and generated by sliding tribocorrosion, a variable number of larger, irregular nano or micron scale particles with a higher Feret ratio were present and composed of chromium and cobalt with the addition of titanium and vanadium or predominantly titanium, indicating formation at the adapter sleeve-male neck taper interface by mechanically assisted fretting/crevice corrosion and possibly by abrasion for the titanium particles, as described in a study of a MoM LHTHA implant with metallic adapter sleeve.[42] The contribution of a second metal-on-metal surface to the corrosive wear debris is not trivial, since it can significantly increase the oxidative stress in the macrophages, causing exfoliation of a larger number of predominantly necrotic macrophages with the release of secondary particles and subsequent modification of the lubricating tribolayer with potential acceleration of the wear process and increased occurrence of ALTRs as previously reported.[40]

In the Non-MoM DMNTHA group, only scattered and irregular nano-size particle aggregates were identified in the macrophages. Larger particles detected in multinucleated giant cells were formed by agglomeration of circular corrosion particles composed of co-localized chromium, cobalt, molybdenum and titanium, indicating formation by mechanically assisted fretting and crevice formation at the neck distal taper interface with the femoral stem female taper. An additional source of particles of uncertain clinical significance can also be the recently described inflammatory cell induced corrosion.[43,44] Our analysis is supported by the EDS examination of corroded areas of the male neck taper in the retrieval study of the same implant showing similar metal elements.[30] ALTR associated with corrosion at the femoral neck-body junction in a dual-taper stem with a cobalt-chromium modular neck has been reported previously[14,45–47] with both neck and stem components contributing to the wear, although loss of substance has been predominantly reported from the male taper.[48] In contrast to the amorphous nature of the particles of the MoM bearing surface groups, they showed a crystalline structure by XRD analysis, a

finding of undetermined biological significance. Iron was detected without co-localization in several samples of all three classes of implants, most likely generated from blood products observed at conventional histological examination. The observation of numerous mast cells in toluidine blue stained semi-thin sections of several samples of the Non-MoM DMNTHA group near deposits of wear particulate material often associated with eosinophils is suggestive of a peculiar hypersensitivity/allergic reaction to complex corrosion wear products of this type of implant. The electron dense matrix surrounding large aggregates of corrosion wear particles is indicative of a possible interaction with proteins with strong affinity for metal elements or ions and warrants further investigation.

The correlation of particle characteristics with statistically significant differences in the histological findings observed in this series of 53 cases and for comparison in the full series of 285 cases of the three groups previously reported[40] shows that the complexity of the morphology and composition of wear particles can be more important than the total particle burden in the occurrence and severity of the ALTR for two main reasons: (a) The complexity of the composition of wear particles correlates with the histological parameters of severity of the adverse reaction, such as soft tissue necrosis, high grade macrophagic and lymphocytic infiltrate, and histological patterns. This correlation indicates that the Non-MoM DMNTHA group with the lowest total burden and the highest particle composition complexity shows the most severe reaction compared to the two MoM groups with less severe reaction, with the HRA group significantly less than the LHTHA group, implicating higher immunogenicity/toxicity of the particles generated at the cone/taper interface; (b) The histological findings are also corroborated by the observation of a significantly shorter time of implantation for the Non-MoM DMNTHA group compared to the other two MoM groups, 28 months *versus* 48 months ($p < 0.001$) in the HRA group and 60 months ($p < 0.001$) in the THA group.

Further analysis will be necessary to assess the importance of nano-size particles and their composition for their effect on bone forming cells and their progenitors, the bone marrow residing mesenchymal stromal cells which might determine the rate of occurrence of acetabular and/or femoral osteolysis at mid-term and long-term implantation time,[49] a late adverse effect which might become a leading mechanism of failure in the near future.[40]

Our particle analysis provides also useful indications for future pre-marketing testing of the implant tribology and toxicological analysis *in vitro* and or *in vivo* of the projected particle wear for the prediction of the biological response as recently reviewed[50]: (1) The majority of the pre-marketing studies of orthopedic implants have focused on the wear generated at the bearing surface, with scant o no data provided for the metal-on-metal head–neck and/or neck-stem junctions, missing crucial data on additional wear particles formed at these surfaces; (2) The complexity of the morphology and the composition of the intracellular particles *in vivo* is difficult to predict by *in vitro* testing, usually with oversimplification of the particle characteristics; (3) Toxicological studies have used particles of standard size or generated by mechanical testing and composed of one or at the most two metallic elements, where the occurrence *in vivo* can be more complex with co-localization of several metals in the same particles, as shown in our analysis of the Non-MoM DMNTHA group which had an unexpected high failure rate after a short time of implantation[51]; (4) Intracellular particle nano-analysis *in vivo* coupled with a detailed histological examination of the periprosthetic tissue can be the first step to confirm or disprove the pre-marketing *in vitro* and *in vivo* testing and provide information on the interaction between wear particles and the host immune system.[52]

We acknowledge several limitations of our study: first, the tissues were retrieved at the time of revision, which was variable from the initial surgery, even within each implant group; second, it was not possible to distinguish between primary wear particles and secondary particles phagocytized after their release from apoptotic macrophages and/or tissue necrosis; third, the morphological and elemental analysis of the particles did not provide information about their tridimensional structure and possible association with specific protein component(s) which could be a critical factor for the initiation of the immunologic inflammatory reaction, as previously reported[53–55].

In conclusion, the nano-analysis of *in vivo* intracellular wear particles of three different classes of hip implants demonstrated that the particle physical characteristics and metal composition are highly consistent in each class and correlate with histological differences in quantitative and qualitative aspects of the ALTR, indicating that the immunogenicity and toxicity of the particles is a leading factor in the onset and severity of the reaction. We also showed that the analysis can provide guidance for toxicological studies on wear particles and a better understanding of how the wear products initiate the distinct host responses involved in the onset and development of ALTR. We hope that this body of information could lead to the development of effective strategies to prevent or limit the occurrence of ALTR and the need for revision surgery in the remaining large population at risk.

Acknowledgment

We would like to acknowledge the surgeons of the Adult Reconstruction and Joint Replacement Service at the Hospital for Special Surgery for providing periprosthetic tissue for this study; Irina Shuleshko and Yana Bronfman, Hospital for Special Surgery, for histological processing and slide preparation; and Randal McKenzie of McKenzie Illustrations for preparation of the graphic illustrations.

Appendix A. Supplementary Data

Supplementary data to this article can be found online at doi:10.1016/j.nano.2016.11.003.

References

1. Fricka KB, Ho H, Peace WJ, Engh Jr CA. Metal-on-metal local tissue reaction is associated with corrosion of the head taper junction. *J Arthroplast* 2012;**27**:26-31.e1, http://dx.doi.org/10.1016/j.arth.2012.03.019.

2. MacDonald SJ. Metal-on-metal total hip arthroplasty: the concerns. *Clin Orthop Relat Res* 2004;**429**:86-93.
3. Medley JB, Chan FW, Krygier JJ, Bobyn JD. Comparison of alloys and designs in a hip simulator study of metal on metal implants. *Clin Orthop Relat Res* 1996;**329**:S148-59 [Suppl].
4. Sieber HP, Rieker CB, Kottig P. Analysis of 118 second-generation metal-on-metal retrieved hip implants. *J Bone Joint Surg (Br)* 1999;**81**(1):46-50.
5. Lachiewicz PF. Metal-on-metal hip resurfacing: a skeptic's view. *Clin Orthop Relat Res* 2007;**465**:86-91.
6. McMinn DJ, Daniel J, Ziaee H, Pradhan C. Indications and results of hip resurfacing. *Int Orthop* 2011;**35**(2):231-7, http://dx.doi.org/10.1007/s00264-010-1148-8.
7. Amstutz HC, Grigoris P. Metal on metal bearings in hip arthroplasty. *Clin Orthop Relat Res* 1996;**329**:S11-34 [Suppl].
8. Srinivasan A, Jung E, Levine BR. Modularity of the femoral component in total hip arthroplasty. *J Am Acad Orthop Surg* 2012;**20**(4):214-22, http://dx.doi.org/10.5435/JAAOS-20-04-214.
9. Werner PH, Ettema HB, Witt F, Morlock MM, Verheyen CC. Basic principles and uniform terminology for the head–neck junction in hip replacement. *Hip Int* 2015;**25**(2):115-9, http://dx.doi.org/10.5301/hipint.5000204.
10. Lombardi Jr AV, Barrack RL, Berend KR, Cuckler JM, Jacobs JJ, Mont MA, et al. The hip society: algorithmic approach to diagnosis and management of metal-on-metal arthroplasty. *J Bone Joint Surg (Br)* 2012;**94**(11 Suppl A):14-8, http://dx.doi.org/10.1302/0301-620X.94B11.30680.
11. Bozic KJ, Kurtz S, Lau E, Ong K, Chiu V, Vail TP, et al. The epidemiology of bearing surface usage in total hip arthroplasty in the United States. *J Bone Joint Surg Am* 2009;**91**(7):1614-20, http://dx.doi.org/10.2106/JBJS.H.01220.
12. Lehil MS, Bozic KJ. Trends in total hip arthroplasty implant utilization in the United States. *J Arthroplast* 2014;**29**(10):1915-8, http://dx.doi.org/10.1016/j.arth.2014.05.017.
13. Witt F, Bosker BH, Bishop NE, Ettema HB, Verheyen CC, Morlock MM. The relation between titanium taper corrosion and cobalt-chromium bearing wear in large-head metal-on-metal total hip prostheses: a retrieval study. *J Bone Joint Surg Am* 2014;**96**(18):e157, http://dx.doi.org/10.2106/JBJS.M.01199.
14. Cooper HJ, Urban RM, Wixson RL, Meneghini RM, Jacobs JJ. Adverse local tissue reaction arising from corrosion at the femoral neck-body junction in a dual-taper stem with a cobalt-chromium modular neck. *J Bone Joint Surg Am* 2013;**95**(10):865-72, http://dx.doi.org/10.2106/JBJS.L.01042.
15. Munro JT, Masri BA, Duncan CP, Garbuz DS. High complication rate after revision of large-head metal-on-metal total hip arthroplasty. *Clin Orthop Relat Res* 2014;**472**(2):523-8, http://dx.doi.org/10.1007/s11999-013-2979-6.
16. Mokka J, Mäkelä KT, Virolainen P, Remes V, Pulkkinen P, Eskelinen A. Cementless total hip arthroplasty with large diameter metal-on-metal heads: short-term survivorship of 8059 hips from the Finnish arthroplasty register. *Scand J Surg* 2013;**102**(2):117-23, http://dx.doi.org/10.1177/1457496913482235.
17. Mao X, Tay GH, Godbolt DB, Crawford RW. Pseudotumor in a well-fixed metal-on-polyethyleneuncemented hip arthroplasty. *J Arthroplast* 2012;**27**(3):493.e13-7, http://dx.doi.org/10.1016/j.arth.2011.07.015.
18. Wyles CC, Van Demark III RE, Sierra RJ, Trousdale RT. High rate of infection after aseptic revision of failed metal-on-metal total hip arthroplasty. *Clin Orthop Relat Res* 2014;**472**(2):509-16, http://dx.doi.org/10.1007/s11999-013-3157-6.
19. Beaver Jr WB, Fehring TK. Abductor dysfunction and related sciatic nerve palsy, a new complication of metal-on-metal arthroplasty. *J Arthroplast* 2012;**27**(7):1414.e13-5, http://dx.doi.org/10.1016/j.arth.2011.11.002.
20. Kayani B, Rahman J, Hanna SA, Cannon SR, Aston WJ, Miles J. Delayed sciatic nerve palsy following resurfacing hip arthroplasty caused by metal debris. *BMJ Case Rep* 2012;**2012**, http://dx.doi.org/10.1136/bcr-2012-006856 [pii: bcr2012006856].
21. Haddad FS, Thakrar RR, Hart AJ, Skinner JA, Nargol AV, Nolan JF, et al. Metal-on-metal bearings: the evidence so far. *J Bone Joint Surg (Br)* 2011;**93**(5):572-9, http://dx.doi.org/10.1302/0301-620X.93B4.26429.
22. Matharu GS, Mellon SJ, Murray DW, Pandit HG. Follow-up of metal-on-metal hip arthroplasty patients is currently not evidence based or cost effective. *J Arthroplast* 2015;**30**(8):1317-23, http://dx.doi.org/10.1016/j.arth.2015.03.009.
23. Willert HG, Buchhorn GH, Fayyazi A, Flury R, Windler M, Köster G, et al. Metal-on-metal bearings and hypersensitivity in patients with artificial hip joints. A clinical and histomorphological study. *J Bone Joint Surg Am* 2005;**87**(1):28-36.
24. Natu S, Sidaginamale RP, Gandhi J, Langton DJ, Nargol AV. Adverse reactions to metal debris: histopathological features of periprosthetic soft tissue reactions seen in association with failed metal on metal hip arthroplasties. *J Clin Pathol* 2012;**65**(5):409-18, http://dx.doi.org/10.1136/jclinpath-2011-200398.
25. Grammatopoulos G, Pandit H, Kamali A, Maggiani F, Glyn-Jones S, Gill HS, et al. The correlation of wear with histological features after failed hip resurfacing arthroplasty. *J Bone Joint Surg Am* 2013;**95**(12):e81, http://dx.doi.org/10.2106/JBJS.L.00775.
26. Perino G, Ricciardi BF, Jerabek SA, Martignoni G, Wilner G, Maass D, et al. Implant based differences in adverse local tissue reaction in failed total hip arthroplasties: a morphological and immunohistochemical study. *BMC Clin Pathol* 2014;**14**:39, http://dx.doi.org/10.1186/1472-6890-14-39.
27. Lohmann CH, Meyer H, Nuechtern JV, Singh G, Junk-Jantsch S, Schmotzer H, et al. Periprosthetic tissue metal content but not serum metal content predicts the type of tissue response in failed small-diameter metal-on-metal total hip arthroplasties. *J Bone Joint Surg Am* 2013;**95**(17):1561-8, http://dx.doi.org/10.2106/JBJS.L.01273.
28. Watters TS, Cardona DM, Menon KS, Vinson EN, Bolognesi MP, Dodd LG. Aseptic lymphocyte-dominated vasculitis-associated lesion: a clinicopathologic review of an underrecognized cause of prosthetic failure. *Am J Clin Pathol* 2010;**134**(6):886-93, http://dx.doi.org/10.1309/AJCPLTNEUAH8XI4W.
29. Higgs GB, Hanzlik JA, MacDonald DW, Gilbert JL, Rimnac CM, Kurtz SM. Implant research center writing committee. Is increased modularity associated with increased fretting and corrosion damage in metal-on-metal total hip arthroplasty devices?: a retrieval study. *J Arthroplast* 2013;**28**(8 Suppl):2-6, http://dx.doi.org/10.1016/j.arth.2013.05.040.
30. De Martino I, Assini JB, Elpers ME, Wright TM, Westrich GH. Corrosion and fretting of a modular hip system: a retrieval analysis of 60 rejuvenate stems. *J Arthroplast* 2015;**30**(8):1470-5, http://dx.doi.org/10.1016/j.arth.2015.03.010.
31. Huber M, Reinisch G, Trettenhahn G, Zweymüller K, Lintner F. Presence of corrosion products and hypersensitivity-associated reactions in periprosthetic tissue after aseptic loosening of total hip replacements with metal bearing surfaces. *Acta Biomater* 2009;**5**(1):172-80, http://dx.doi.org/10.1016/j.actbio. 2008.07.032.
32. Mittal S, Revell M, Barone F, Hardie DL, Matharu GS, Davenport AJ, et al. Lymphoid aggregates that resemble tertiary lymphoid organs define a specific pathological subset in metal-on-metal hip replacements. *PLoS One* 2013;**8**(5):e63470, http://dx.doi.org/10.1371/journal.pone.0063470.
33. Campbell P, Ebramzadeh E, Nelson S, Takamura K, De Smet K, Amstutz HC. Histological features of pseudotumor-like tissues from metal-on-metal hips. *Clin Orthop Relat Res* 2010;**468**(9):2321-7, http://dx.doi.org/10.1007/s11999-010-1372-y.
34. Catelas I, Medley JB, Campbell PA, Huk OL, Bobyn JD. Comparison of *in vitro* with *in vivo* characteristics of wear particles from metal–metal hip implants. *J Biomed Mater Res B Appl Biomater* 2004;**70**(2):167-78.
35. Hart AJ, Quinn PD, Sampson B, Sandison A, Atkinson KD, Skinner JA, et al. The chemical form of metallic debris in tissues surrounding metal-on-metal hips with unexplained failure. *Acta Biomater* 2010;**6**(11):4439-46, http://dx.doi.org/10.1016/j.actbio.2010.06.006.

36. Xia Z, Kwon YM, Mehmood S, Downing C, Jurkschat K, Murray DW. Characterization of metal-wear nanoparticles in pseudotumor following metal-on-metal hip resurfacing. *Nanomedicine* 2011;**7**(6):674-81, http://dx.doi.org/10.1016/j.nano.2011.08.002.
37. Keegan GM, Learmonth ID, Case CP. A systematic comparison of the actual, potential, and theoretical health effects of cobalt and chromium exposures from industry and surgical implants. *Crit Rev Toxicol* 2008;**38**(8):645-74, http://dx.doi.org/10.1080/10408440701845534.
38. Scientific Committee on Emerging and Newly Identified Health Risks (SCENIHR). *Opinion on the Safety of Metal-On-Metal Joint Replacements with a Particular Focus on Hip Implants*; 20141-64.
39. Bertazzo S, Gentleman E, Cloyd KL, Chester AH, Yacoub MH, Stevens MM. Nano-analytical electron microscopy reveals fundamental insights into human cardiovascular tissue calcification. *Nat Mater* 2013;**12**(6):576-83.
40. Ricciardi BF, Nocon AA, Jerabek SA, Wilner G, Kaplowitz E, Goldring SR, et al. Histopathological characterization of corrosion product associated adverse local tissue reaction in hip implants: a study of 285 cases. *BMC Clin Pathol* 2016;**16**:3, http://dx.doi.org/10.1186/s12907-016-0025-9.
41. Madl AK, Liong M, Kovochich M, Finley BL, Paustenbach DJ, Oberdörster G. Toxicology of wear particles of cobalt-chromium alloy metal-on-metal hip implants part I: physicochemical properties in patient and simulator studies. *Nanomedicine* 2015;**11**(5):1201-15, http://dx.doi.org/10.1016/j.nano.2014.12.005.
42. Meyer H, Mueller T, Goldau G, Chamaon K, Ruetschi M, Lohmann CH. Corrosion at the cone/taper interface leads to failure of large-diameter metal-on-metal total hip arthroplasties. *Clin Orthop Relat Res* 2012;**470**(11):3101-8, http://dx.doi.org/10.1007/s11999-012-2502-5.
43. Gilbert JL, Sivan S, Liu Y, Kocagöz SB, Arnholt CM, Kurtz SM. Direct *in vivo* inflammatory cell-induced corrosion of CoCrMo alloy orthopedic implant surfaces. *J Biomed Mater Res A* 2015;**103**(1):211-23, http://dx.doi.org/10.1002/jbm.a.35165.
44. Di Laura A, Hothi HS, Meswania JM, Whittaker RK, de Villiers D, Zustin J, et al. Clinical relevance of corrosion patterns attributed to inflammatory cell-induced corrosion: a retrieval study. *J Biomed Mater Res B Appl Biomater* 2015, http://dx.doi.org/10.1002/jbm.b.33540.
45. Gill IP, Webb J, Sloan K, Beaver RJ. Corrosion at the neck-stem junction as a cause of metal ion release and pseudotumour formation. *J Bone Joint Surg (Br)* 2012;**94**(7):895-900, http://dx.doi.org/10.1302/0301-620X.94B7.29122.
46. Kop AM, Swarts E. Corrosion of a hip stem with a modular neck taper junction: a retrieval study of 16 cases. *J Arthroplast* 2009;**24**(7):1019-23, http://dx.doi.org/10.1016/j.arth.2008.09.009.
47. Pivec R, Meneghini RM, Hozack WJ, Westrich GH, Mont MA. Modular taper junction corrosion and failure: how to approach a recalled total hip arthroplasty implant. *J Arthroplast* 2014;**29**(1):1-6, http://dx.doi.org/10.1016/j.arth.2013.08.026.
48. Buente D, Huber G, Bishop N, Morlock M. Quantification of material loss from the neck piece taper junctions of a bimodular primary hip prosthesis. A retrieval study from 27 failed rejuvenate bimodular hip arthroplasties. *Bone Joint J* 2015;**97-B**(10):1350-7, http://dx.doi.org/10.1302/0301-620X.97B10.35342.
49. Rakow A, Schoon J, Dienelt A, Thilo J, Textor M, Duda G, et al. Influence of particulate and dissociated metal-on-metal hip endoprosthesis wear on mesenchymal stromal cells *in vivo* and *in vitro*. *Biomaterials* 2016;**98**:31-40, http://dx.doi.org/10.1016/j.biomaterials.2016.04.023.
50. Nine MJ, Choudhury D, Hee AC, Mootanah R, Osman NAA. Wear debris characterization and corresponding biological response: artificial hip and knee joints. *Materials* 2014;**7**:980-1016, http://dx.doi.org/10.3390/ma7020980.
51. Nawabi DH, Do HT, Ruel A, Lurie B, Elpers MA, Wright T, et al. Comprehensive analysis of a recalled modular total hip system and recommendations for management. *J Bone Joint Surg Am* 2016;**98**:40-7, http://dx.doi.org/10.2016/jbjs.N.01121.
52. Munir S, Oliver RA, Zicat B, Walter WL, Walter WK, Walsh WR. The histological and elemental characterisation of corrosion particles from taper junctions. *Bone Joint Res* 2016;**5**:370-8, http://dx.doi.org/10.1302/2046–3758.59.2000507.
53. Mathew MT, Nagelli C, Pourzal R, Fischer A, Laurent MP, Jacobs JJ, et al. Tribolayer formation in a metal-on-metal (MoM) hip joint: an electrochemical investigation. *J Mech Behav Biomed Mater* 2014;**29**:199-212, http://dx.doi.org/10.1016/j.jmbbm.2013.08.018.
54. Reddy A, Caicedo MS, Samelko L, Jacobs JJ, Hallab NJ. Implant debris particle size affects serum protein adsorption which may contribute to particle size-based bioreactivity differences. *J Long-Term Eff Med Implants* 2014;**24**(1):77-88.
55. Loeschner K, Harrington CF, Kearney JL, Langton DJ, Larsen EH. Feasibility of asymmetric flow field-flow fractionation coupled to ICP-MS for the characterization of wear metal particles and metalloproteins in biofluids from hip replacement patients. *Anal Bioanal Chem* 2015;**407**(16):4541-54, http://dx.doi.org/10.1007/s00216-015-8631-4.